International Journal of Rail Transportation

ISSN: (Print) (Online) Journal homepage: https://www.tandfonline.com/loi/tjrt20

Investigating the re-adhesion performance of locomotives with bogie frame suspension driving system

Guosong Wu, Longjiang Shen & Yuan Yao

To cite this article: Guosong Wu, Longjiang Shen & Yuan Yao (2023) Investigating the re-adhesion performance of locomotives with bogie frame suspension driving system, International Journal of Rail Transportation, 11:2, 267-288, DOI: 10.1080/23248378.2022.2075945

To link to this article: https://doi.org/10.1080/23248378.2022.2075945

Published online: 22 May 2022.

INTERNATIONAL JOURNAL OF RAIL TRANSPORTATION
2023, VOL. 11, NO. 2, 267–288
https://doi.org/10.1080/23248378.2022.2075945

Investigating the re-adhesion performance of locomotives with bogie frame suspension driving system

Guosong Wu[a], Longjiang Shen[b,c] and Yuan Yao[a]

[a]State Key Laboratory of Traction Power, Southwest Jiaotong University, Chengdu, People's Republic of China; [b]Bogie R&D Department, CRRC Zhuzhou Electric Locomotive Co., Ltd, Zhuzhou, People's Republic of China; [c]State Key Laboratory of Heavy Duty AC Drive Electric Locomotive Systems Integration, CRRC Zhuzhou Electric Locomotive Ltd., Zhuzhou, People's Republic of China

ABSTRACT

The readhesion performance and driving system dynamics of locomotives with bogie frame suspension driving system were investigated. To investigate the driving system's vibration characteristics in the adhesion saturation state and the influencing factors for locomotive's readhesion performance, a train dynamic model was established. According to the simulation results, increasing the torsional stiffness of six-bar double hollow shaft coupling and adopting the traction motor with hard mechanical characteristics are beneficial for the locomotive's readhesion performance. Besides, increasing the motor suspension stiffness within a certain range is advantageous. Moreover, resonance analysis was conducted, which indicated that the resonance of the driving system occurs if the natural frequency of wheelset's longitudinal vibration is close to the rotary vibration natural frequency or its frequency doubling. Reasonable matching of primary longitudinal stiffness and six-bar double hollow shaft coupling stiffness is emphasized.

ARTICLE HISTORY
Received 29 December 2021
Revised 5 May 2022
Accepted 6 May 2022

KEYWORDS
Heavy-haul locomotive; bogie frame suspension; driving system; readhesion performance; stick-slip vibration

1. Introduction

With the rapid development of heavy-haul transportation, high-power locomotives have become more and more popular all over the world. Considering that the locomotive's traction and braking force are not only produced but also strictly limited by the wheel-rail adhesion, the power of locomotives cannot be increased infinitely. Therefore, the wheel-rail adhesion has become a key issue to improve the traction and braking capacity of locomotives. A great number of experimental and simulation results show that the wheel-rail adhesion increases linearly with the increasing creepage in the small creep zone and then the adhesion increases nonlinearly and reaches the adhesion limit in the large creep zone, after that the adhesion enters the sliding area and decreases with the increase of creepage [1–3], which is known as the negative slope characteristics of wheel-rail adhesion. The wheel-rail adhesion saturation and negative slope characteristics can cause complex dynamic problems, such as the scratch of wheel tread and rail surface and the wheel polygonal wear, and even threaten the safety of locomotives in operation [4–7]. The research on the dynamic characteristics of locomotives in adhesion saturation can be conducive to improving the traction effort and reducing the dynamic force exerted on the locomotive driving system by reasonably matching the bogie structural parameters, driving system parameters, and electrical parameters.

CONTACT Yuan Yao yyuan8848@163.com State Key Laboratory of Traction Power, Southwest Jiaotong University, Chengdu 610031, People's Republic of China

Large traction effort is needed for the heavy-haul locomotive during the process of starting and uphill, causing the wheel-rail adhesion close to the adhesion limit. Whereas the wheel-rail adhesion cannot be maintained at the peak value, it is easy to enter the sliding zone due to the negative slope of adhesion. Besides, if there is a third medium on the rail surface, such as rain, snow, leaves, oil, and so on, the adhesion coefficient will decrease and makes it easier to enter the sliding zone [8,9], which may lead to the complex dynamic behaviour of the locomotive driving system. A great number of research studies on locomotive driving system dynamics have been conducted by means of simulation and experiment. Hirotsu et al. [10] studied the self-excited vibration during slippage for the parallel Cardan drives used in electric railcars by theoretical analysis and experimental tests and clarified the measures to suppress self-excited vibration by means of increasing the stiffness, as well as damping of the driving system structure. Muller and Kogel [11] analysed the wheelset roll-slip vibration on condition that the contact conditions for two wheels of a wheelset are different, and the influence of mechanical design parameters on roll-slip vibration is demonstrated. Wu [12] analysed the stick-slip vibration stability of the frame-mounted motor driving system by simulation and found that the reasonable matching of driving system parameters as well as traction motor performance is conducive to improving the stick-slip vibration stability. Sun [13] established a mechanical-electrical dynamic model and analysed the influencing factors of the stick-slip vibration of locomotives. Besides, Sun proposed that the reasonable matching of power and transmission system, mechanical system, and control system is the design principle for high adhesion locomotives. Polach [14,15] developed a fast wheel-rail force calculation code, in which the negative slope characteristics as well as the effects of different rail adhesion conditions are taken into consideration. Michael Lata [16,17] simulated the dynamics of a torsion system of a railway driving vehicle and conducted the experiment that involves the transient phenomenon for the wheelset exceeding the adhesion limit. Besides, the main frequency of the driving system was analysed based on the measured acceleration signals, and it showed the coupling phenomena between rotational and vertical movements of the driving system during the wheelset sliding. Liu et al. [18] investigated the track wear damage resulting from the changes in friction conditions and compared the transient dynamic oscillation of wear between AC and DC electric drive locomotives. Chen et al. [19,20] established the locomotive–track coupled vertical dynamics model with gear transmissions, the effects of gear transmissions on dynamic performance of locomotives under traction and braking conditions are investigated, and the dynamic investigation of traction motor bearing has been conducted by Liu and Chen et al. [21,22]. Ren et al. [23] developed a rigid-flexible coupling dynamics model for railway vehicles including the flexible gear meshing model to investigate the effects of gear transmission on the dynamics of high-speed vehicles. Huang et al. [24] discussed the super-harmonic responses and the stability of the gear transmission system for high-speed train under stick-slip oscillation. Spiryagin et al. [25–29] have performed some related research and obtained some remarkable accomplishments. A co-simulation model including mechanical systems, power systems, traction machines, and traction algorithms was established to improve the precision and efficiency of simulation results, and some traction control strategies were investigated and verified. Yao et al. [30–32] mainly focus on the stick-slip vibration of locomotives with a nose-suspended motor, innovatively proposed the concept of mean and dynamic slip rate, and clarified the mechanism of stick-slip vibration of the locomotive driving system. In addition, the reasonable matching of longitudinal axle guidance stiffness and the motor suspension stiffness is emphasized to avoid resonance when stick-slip vibration occurs.

At present, the bogie frame suspension driving system has been widely used in high-speed locomotives. However, there are more elastic connections in the bogie frame suspension driving system as a result of adopting the six-bar double hollow shaft coupling, which is unfavourable for the stick-slip vibration and the readhesion performance of the locomotive, the heavy-haul locomotive with a bogie frame suspension driving system was taken as the research object, and a dynamic model of train system including a detailed locomotive model and a simplified vehicle model was established by SIMPACK, in which the mechanical characteristics of the asynchronous motor and gear transmission were taken into consideration. Then, the stick-slip vibration characteristics of the driving system were studied, and the influencing factors of locomotive's readhesion performance were analysed by simulation. At last, more attention was paid to the structural resonance due to the unreasonable parameter matching when the stick-slip vibration occurs, which should be avoided during the process of locomotive design.

2. Theory of stick-slip vibration

2.1. Stick-slip vibration mechanism

As is well known, the rigid wheel slide occurs rather than just elastic creep during the process of locomotive driving and braking. To express the slippage in a more physical sense, the slip in locomotive's driving dynamics is defined as follows:

$$S = \frac{v - \omega r}{v} = 1 - \frac{\left(\omega_0 + \dot{\theta}\right) r}{v_0 + \dot{x}} \tag{1}$$

where v is the instantaneous speed of the wheelset; v_0 is the mean speed; ω is the instantaneous angular velocity; ω_0 is the mean angular velocity; $\dot{\theta}$ and $\dot{x}$ are the rotary and longitudinal vibration speed of the wheelset, respectively; and r is the radius of wheel. It is noteworthy that s is a negative value under the driving condition, and thus, its absolute value is adopted in the following analysis.

As a dynamic variable, the slip s can be written as

$$s = s_0 + ds, \tag{2}$$

where S_0 is the mean slip and ds is the dynamic slip. S_0 is not only dependent on the braking or traction effort but also restricted by the wheel-rail adhesion condition. The magnitude of ds is regarded to be related to the vibration energy, as well as the stiffness and damping corresponding to the elastic connections in the wheelset driving system structure.

According to Ref. [16], the cooperation of adhesive characteristics with traction motor characteristics can be divided into three types, which are described as subcritical cooperation, critical cooperation, and supercritical cooperation, respectively. Considering that the mechanical characteristics of asynchronous motor are hard, the typical subcritical cooperation is considered, in which the motor torque curve crosses the new adhesive characteristics in its negative slope parts when the

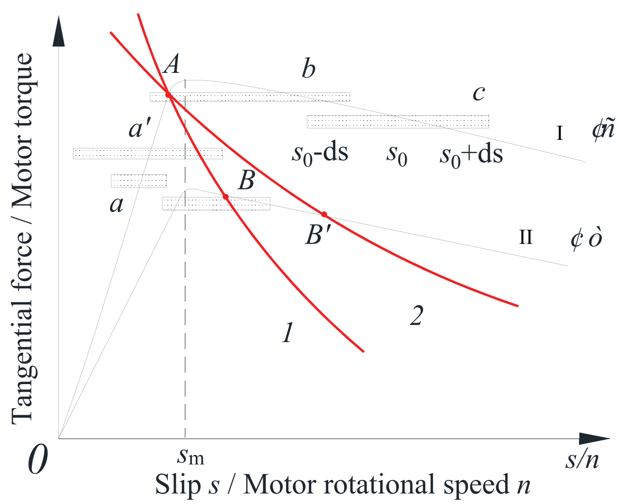

Figure 1. Mechanism analysis of stick-slip vibration.

adhesion condition becomes worse under the condition of high traction effort. As shown in Figure 1, the red curves represented by Arabic numerals *1* and *2* describe the different mechanical characteristics of the asynchronous traction motor, and the black curves represented by Roman numerals *I* and *II* describe the adhesive characteristics corresponding to different adhesion conditions. There are three typical states for the wheel-rail contact in the driving condition, which are called the stick state represented by symbol "*a*,“ the stick-slip state represented by symbol "*b*,“ and the slip state represented by symbol "*c*“ in Figure 1. It should be noted that the stick-slip state is unstable, and its further development depends on the system state.

Assume that the locomotive is operating at point *A*, which is the intersection of the adhesion characteristics curve *I* and the motor characteristics curve *1*. At a certain moment, the adhesion condition decreases due to the third medium, such as oil pollution, fallen leaves, and so on. Thus, the adhesion characteristics curve changes to curve *II*, which intersects with the motor mechanical characteristics curve at point *B*, causing the wheelset to accelerate to slide on the rail surface without any control measures. During the process of adhesion decreasing and recovery, it is easier to reach the stick-slip state from the slip state if the structural stiffness and damping of the driving system are unreasonable. If the readhesion performance of the locomotive is good, the adhesion can be quickly restored; otherwise, the unstable self-excited vibration may occur, which will not only cause the traction effort that cannot be made full use of but also lead to the damage of driving system components.

It is worth noting that the motor mechanical characteristics of curve *2* are softer than those of curve *1*, and thus, the slip corresponding to the intersection of the mechanical characteristics curve and the new adhesion characteristics curve is larger than that of curve *1*. As a result, the larger input energy makes it easier to change the wheelset from slippage to stick-slip. Similarly, the conditions *b* and *c* can be compared and explained. Besides, considering that the structural stiffness and damping of the wheelset driving system are smaller and the vibration scope of slip is comparatively wider, thus, it is more quick to reach the stick-slip state under condition *a'* compared with *a*.

It can be concluded that reducing the average and dynamic slip are the two most basic strategies to improve the readhesion performance of locomotives. That is to say, there are many factors affecting the locomotive's readhesion ability, such as rail surface condition, locomotive structural parameters, electric drive system, motor mechanical characteristics and so on. In the view of bogie structure design, it is necessary to optimize the structural stiffness and damping of the driving system to reduce the vibration range of slip.

2.2. Wheelset longitudinal vibration

Assuming that the motor torque is constant and ignoring the damping of locomotive's driving system, the graphic analysis of wheelset's longitudinal and rotational coupling vibration is conducted, as shown in Figure 2.

Positive damping acts on the wheelset and results in the decrease of system energy when the slip is located in the *OA* section, while it is located in the *AB* section, the system energy increases because of the negative damping. Consequently, the angular acceleration of the wheelset will be negative when the slip is located in the *OA* section, while the slip is located in the *AB* section, it will be positive. For the longitudinal acceleration of the wheelset, it is positive on condition that the tangential force coefficient is greater than u_0 corresponding to the shaded area in Figure 2 and vice versa. When the stick-slip vibration occurs, the minimum and maximum slip is located on both sides of s_0, which are represented by s_1 and s_2, respectively. Considering that the slip changes in one period of "s_1-s_2-s_1,“ the wheelset's angular acceleration experiences a cycle of "negative-positive-negative,“ and thus, the wheelset's angular velocity experiences a cycle of "decrease-increase-decrease.“ While for the wheelset's longitudinal acceleration, it will be in a "negative-positive-negative-positive-negative“ cycle, certainly, the wheelset's longitudinal velocity experiences a cycle

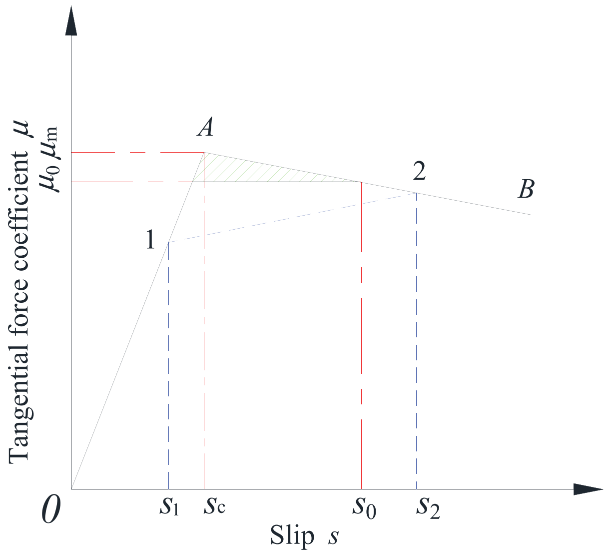

Figure 2. Analysis of wheelset's longitudinal and rotational coupling vibration.

of "decrease-increase-decrease-increase-decrease." It can be concluded that the rotary and longitudinal vibrations of the wheelset are coupled by wheel-rail tangential force, resulting in the appearance of some complex frequency components when stick-slip vibration occurs, which implies that resonance may occur if the unreasonable parameter matching is adopted.

3. Dynamic simulation model

3.1. Driving system model

At present, the locomotives in service in China can be roughly divided into two types according to the different suspension modes of the driving system, namely nose-suspended and bogie frame suspension. The former is mainly used for the locomotive with a top speed of 120 km/h, while the latter is suitable for a higher speed level. The nose-suspended has the advantages of a simple structure and large torsional stiffness, which are advantageous for the readhesion ability of locomotive. As for the bogie frame suspension, it has a smaller unsprung mass, and thus, its wheel-rail interaction is better. However, its torsional stiffness is relatively small because there are some elastic connections in the driving system, which is unfavourable for the readhesion performance of the locomotive. In this study, the bogie frame driving system is adopted for heavy-haul locomotives with a top speed of 120 km/h to reduce the unsprung mass and thus to reduce the wheel-rail dynamic forces.

For the nose-suspended, one end of the driving system is held on the axle by rolling bearing and the other end is hung on the frame by the suspender, the equivalent vertical stiffness of which is represented by K_{mz}. The driving system has only one pitch degree of freedom relative to the wheelset. Besides, the motor rotor and pinion are connected by coupling, and the equivalent torsional stiffness is represented by K_r, as shown in Figure 3(a). For the bogie frame suspension, one end of the driving system is mounted on the bogie frame through a rubber sleeve, the equivalent vertical stiffness of which is represented by K_{zc}, and the other end is suspended on the frame through two hanger rods and rubber joints, the equivalent vertical stiffness of which is represented by K_{za}. Besides, a six-bar double hollow shaft coupling is used to transfer the motor torque and to

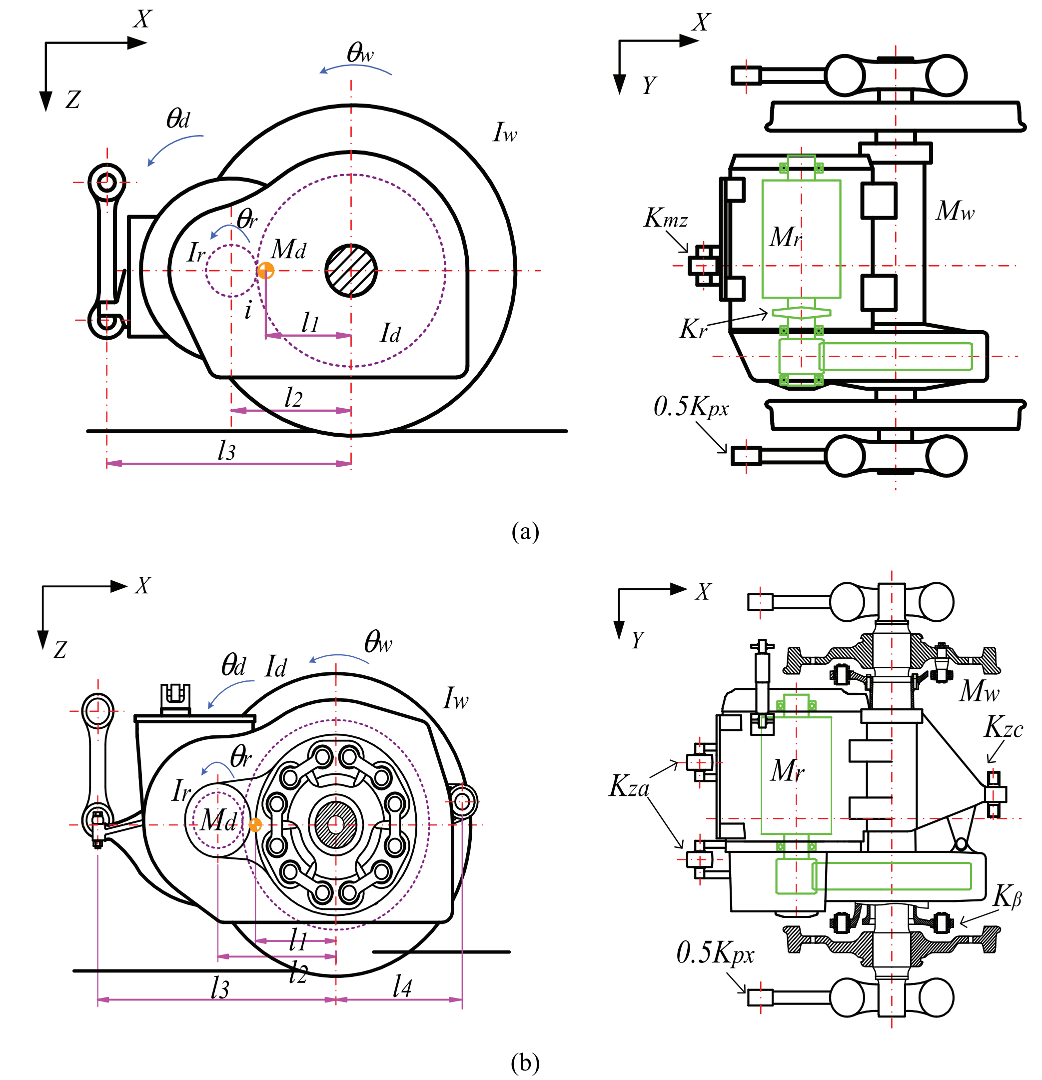

Figure 3. Driving system architectures: (a) nose-suspended and (b) bogie frame suspension.

adapt the relative motion between the driving system and the wheelset, and the equivalent torsional stiffness is K_β, as shown in Figure 3(b). The detailed parameters of the driving system's dynamic model are shown in Table 1.

Considering that there are many elastic connections in the bogie frame suspension architecture, which is unfavourable for the readhesion performance of locomotives, the AC drive electric locomotive with a bogie frame suspension driving system is taken as the research object, the single axle power and the axle load of which are 1200 kW and 30 t, respectively.

3.2. Equivalent torsional stiffness

In order to analyse the torsional vibration of the system with gear transmission, the system parameters of the input or output axis can be equivalent to the same axis according to the equivalence principle. Based on the principle of energy conservation, the equivalent torsional stiffness is as follows:

Table 1. Parameters of the driving system's dynamic model.

Symbol	Physics mean	Value
M_w	Mass of the wheelset (kg)	3138
I_w	Pitch inertia of the wheelset (kg m^2)	440
M_d	Mass of the motor stator (not including rotor of motor) (kg)	3014
I_d	Pitch inertia of motor stator (not including rotor of motor) (kg m^2)	1619
M_r	Mass of the rotor (kg)	650
I_r	Pitch inertia of the rotor (kg m^2)	19.7
l_1	Longitudinal distance from the mass centre of the drive system to the wheelset (mm)	512
l_2	Longitudinal distance from the rotor to the wheelset (mm)	660
l_3	Longitudinal distance from the motor suspension rod to the wheelset (mm)	1165
l_4	Longitudinal distance from the motor reverse suspension rod to the wheelset (mm)	600
K_r	Rotary stiffness of rotor coupling (MN m rad^{-1})	12.6
K_β	Rotary stiffness of six-bar double hollow shaft coupling (MN m rad^{-1})	5.2
K_{px}	Longitudinal axle guidance stiffness (kN mm^{-1})	37.4
i	Transmission ratio of gear transmission	5.722

$$K_{\theta e} = K_\theta \cdot i^2. \tag{3}$$

The electromagnetic torque is applied to the rotor by the motor stator and is transferred to the wheelset via gear transmission and six-bar double hollow shaft transmission device. Considering the pitch degree of freedom of the motor stator relative to the wheelset, the pitch movements of the motor stator occur under the action of driving torque. According to the transmission path of motor torque, the motor rotor, stator, six-bar double hollow shaft coupling, and wheelset are connected in series, and the torsional stiffness can be equivalent to the axle of the wheelset, as shown in Figure 4, where K_{re} and K_{de} represent the torsional stiffness of the motor rotor and stator equivalent to the axle of wheelset, respectively; I_{re} and I_{de} represent the equivalent moment of the inertia of the motor rotor and stator, respectively; T_{re} represents the equivalent motor torque. It should be noted that the K_β can almost be rigid for the nose-suspended driving system, while in the bogie frame suspension driving system, it cannot be ignored, and it is the stiffness of six-bar double hollow shaft coupling.

The pitch stiffness of the motor represented by K_d is dependent on the vertical suspension stiffness represented by K_{za} and K_{zc}, and the longitudinal distance represented by l_3 and l_4, which can be expressed as:

$$K_d = 2K_{za} \cdot l_3^2 + K_{zc} \cdot l_4^2, \tag{4}$$

where l_3 and l_4 represent the longitudinal distances from motor hanging points to the wheelset, as shown in Figure 3(b).

According to Ref. [32], when the rotor rotational speed is equal to 0, the transmission ratio from the pitch movement of the motor stator to the wheelset rotation is as follows:

$$i_{dw} = \frac{i}{i-1}. \tag{5}$$

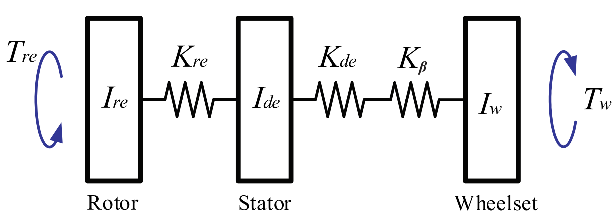

Figure 4. Torsional vibration system model.

According to Equations (3), (4), and (5), the torsional stiffness of the motor rotor and stator equivalent to the axle of the wheelset represented by K_{re} and K_{de}, respectively, can be calculated as follows:

$$K_{re} = K_r \cdot i^2, \tag{6}$$

$$K_{de} = K_d \cdot i_{dw}^2, \tag{7}$$

where K_r is the equivalent coupling stiffness between the rotor and the pinion.

It is worth noting that the equivalent torsional stiffness from the motor rotor to the wheelset equals the coupling stiffness multiplied by the square of the gear transmission ratio, resulting in a great value, and thus, the effects of coupling stiffness between the rotor and the pinion on stick-slip vibration are ignored. Moreover, the equivalent torsional stiffness between the driving system and the wheelset represented by K_t can be equivalent to a composite stiffness of K_{de} and K_β that are in series, and thus, the composite stiffness can be calculated as follows:

$$K_t = \frac{K_{de} \cdot K_\beta}{K_{de} + K_\beta}, \tag{8}$$

where K_β is the equivalent torsional stiffness of six-bar double hollow shaft coupling.

Usually, the calculated K_{de} is much larger than K_β, and thus, the composite stiffness is mainly dependent on K_β. Considering that the six-bar double hollow shaft coupling is the weakness of the bogie frame suspension driving system, more attention should be paid during the process of bogie design.

3.3. Train system dynamic model

A dynamic model of train system is established by SIMPACK, which is composed of one locomotive and fifteen vehicles. Considering the calculation accuracy and efficiency, the locomotive model is established in detail, in which the mechanical characteristics of the asynchronous motor and the gear transmission characteristics are taken into consideration, while the vehicles are simplified as mass blocks with only a longitudinal degree of freedom along the track. The axle loads of vehicles and locomotive are 25 t and 30 t, respectively. Besides, the locomotive is equipped with a B_0-B_0 axle arrangement, and the uniaxial power is 1200 kW. The main parameters of the locomotive dynamic model are shown in Appendix Table A1.

The locomotive model is composed of one car body, two bogie frames, four wheelsets, four hollow shafts, four integrals of motor stator and gearbox, four motor rotors, eight hanger rods for traction motor, two sets of traction devices (each set includes one horizontal traction rod, inclined traction rod, and hanger rod for the traction device), and four sets of two-staged gear transmission systems (each includes one pinion, middle gear, and big gear), so there are forty-five bodies in total. The car body, bogie frame, wheelset, integral of the motor stator, and gearbox each has six degrees of freedom, the hollow shaft has two degrees of freedom to rotate about the x and z-axis, respectively, the hanger rod for the traction motor and traction device has two degrees of freedom to rotate about the x and y-axis, respectively, the horizontal traction rod has two degrees of freedom to rotate about the y and z-axis, respectively, the inclined traction rod has only one degree of freedom to rotate about the y-axis, and the motor rotor, pinion, middle gear, and big gear each has one degree of freedom to rotate about the y-axis, so there are one hundred and twelve degrees of freedom in total. It should be noted that longitudinal, lateral, and vertical directions of track are defined as x, y, and z-axes, respectively.

The primary suspension is composed of round steel springs, primary vertical dampers, and axle-box with triangular pull rod, the three-dimensional stiffness of which are considered to be fully decoupled. The secondary suspension is composed of high round steel springs, secondary vertical dampers, and lateral dampers. The lateral dampers are arranged at both the ends of the bogie frame, which can play the role of anti-hunting motion at the same time. Besides, there are two lateral stops between the car body and the bogie frame to limit the displacement of car body. The traction device adopts the low push-pull double traction rod, which consists of a horizontal traction rod and an inclined traction rod. One end of the horizontal traction rod is installed under the frame traction beam by rubber joint, and the other end is hung on the frame end beam by the suspender. As for the inclined traction rod, one end is connected with the horizontal traction rod by traction pin and the other end is installed on the traction seat through the rubber joint. In the dynamic simulation model, the dampers are simulated by the Maxwell element, and the rubber joints are simulated by bushing force elements that have stiffness and damping in multiple axis directions.

In order to obtain a greater transmission ratio and higher traction effort, the two-staged gear transmission system is adopted. The driving system is composed of an asynchronous motor, a gear box, hanger rods, a pinion, middle gear, big gear, and a six-bar double hollow shaft. The locomotive driving system adopts an integral structure, where the motor and gear box are suspended on the bogie frame by one rubber sleeve and two hanger rods. To attenuate the lateral vibration of the driving system, there are dampers between the bogie frame and the integral of the motor stator and gearbox and there are also stops to limit the displacement of the driving system. Besides, the motor rotor and pinion are connected by coupling, the equivalent torsional stiffness of which is 12.6 MN·m/rad, the wheelset and big gear are combined with six-bar double hollow shaft coupling, which is used to transfer motor torque to the wheelset and to adapt the relative motion between the driving system and wheelset, and the original equivalent torsional stiffness is 5.2 MN m/rad.

The bogie frame suspension driving system dynamic model is shown in Figure 5.

The resistances are acting on the train model, which are composed of the basic resistance and additional ramp resistance. Assuming that the locomotive's traction force and the train resistance are balanced, the train is running in a uniform velocity. The unit weight resistance is given as:

$$w_0 = a + b{\cdot}v + c{\cdot}v^2 + j(\mathrm{N/kN}), \tag{9}$$

where a, b, and c are resistance coefficients used to characterize the basic resistance and the related resistance coefficients for the corresponding locomotive and waggons can be referred to in Ref. [33], and j is the slope of ramp characterizing the additional ramp resistance.

Besides, the vehicles are connected by couplers, and thus, the longitudinal impact caused by traction effort fluctuation is taken into consideration. In this study, the JM3 worn-type wheel tread matching with the standard 60 kg/m rail in China is adopted, and the US 5 class track irregularity is considered. The dynamic model can be used to simulate the dynamic processes during the locomotive's traction operation.

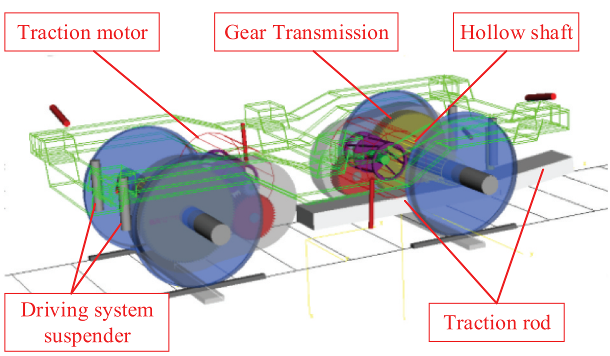

Figure 5. Bogie frame suspension driving system dynamic model.

3.4. Gear transmission

The gear transmission is simulated by the SIMPACK 225 force element based on the actual gear parameters. According to Ref. [34], the meshing stiffness of each tooth pair is calculated, and then the meshing force is obtained by the penetration of the tooth surface involved in meshing and the time-varying meshing stiffness. Considering its high computation efficiency and accuracy, it has been widely used in the dynamic modelling and simulation for the gear transmission system. The meshing stiffness of each tooth pair can be calculated as follows:

$$K' = K'_{th} K_M K_R K_B \cos\beta \tag{10}$$

where K'_{th} represents the theoretical meshing stiffness of each tooth pair; K_M,K_R, and K_B are the correction factors; and β is the helix angle.

The calculated time-varying meshing stiffness can be expressed as:

$$K_{\max} = K' \cdot K_R, \tag{11}$$

$$S_R = K_{min}/K_{max}, \tag{12}$$

$$K(\varphi) = K_{\max} \cdot [1 - (1 - S_R)(\frac{S(\varphi)}{\max(S_1, S_2)})^2], \tag{13}$$

where $K_{\max}$ is the highest value of normal contact stiffness of each tooth pair, which takes place at the pitch point; $K_{\min}$ is the effective meshing stiffness acting on the meshing tooth top relative to the tooth root; S_R is the stiffness ratio; $S(\varphi)$ is the tooth contact path of relative angle; and S_1 and S_2 are the length of entering and away from the meshing route. The parameters of the gear transmission system are shown in Table 2, and the time-varying meshing stiffness curves are shown in Figure 6.

3.5. Coupler connection model

The coupler connection model is composed of a simplified coupler model and draft gears. According to Ref. [35], the coupler draft gears are considered as nonlinear components with hysteresis characteristics, and its resistant force can be expressed as:

$$F(x_c, \Delta v) = \begin{cases} f(x_c) + |f_u(x_c) - f_l(x_c)| sign(\Delta v) & \Delta v \geq ev \\ f(x_c) + \frac{\Delta v}{ev} |f_u(x_c) - f_l(x_c)| sign(\Delta v) & \Delta v \geq ev \end{cases} \tag{14}$$

where f_l (x_c) and f_u (x_c) characterize the loading and unloading characteristics of draft gears, respectively; x_c represents the displacement; Δv represents the change rate of the displacement; and ev represents the switching speed of draft gears. According to the measured data, the characteristics of resistant force for coupler draft gears can be illustrated by the polyline method, as shown in Figure 7.

Table 2. Parameters of the gear transmission system.

Parameters	Value	Parameters	Value
Normal modulus (mm)	9	Number of teeth of medium gear	49
Normal pressure angle (°)	20	Flank width of medium gear (mm)	174
Helix angle (°)	4	Backlash (mm)	0
Number of teeth of small gear	18	Teeth stiffness ratio	0.8
Flank width of small gear (mm)	183	Young's module (GN/m)	210
Number of teeth of large gear	103	Poisson's ratio	0.3
Flank width of large gear (mm)	156	Damping coefficient (kN s/m)	5

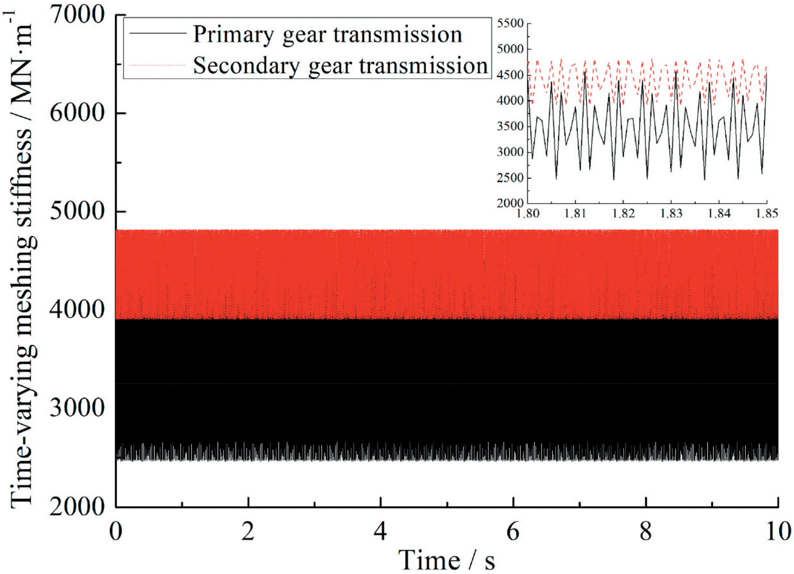

Figure 6. Time-varying meshing stiffness.

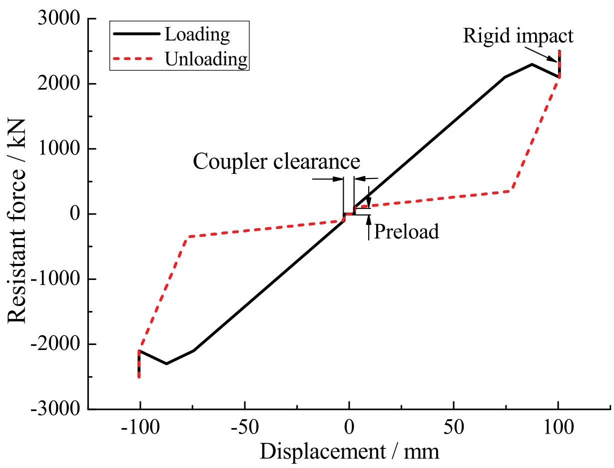

Figure 7. Resistant force characteristics of coupler draft gears.

3.6. Characteristics of wheel-rail adhesion

It is found that the friction coefficient decreases with the increase of relative sliding velocity between the wheel and the rail, that is to say, the wheel-rail adhesion decreases as the creepage increases rather than maintaining at the coulomb friction limit when the creepage exceeds the critical creepage corresponding to the adhesion limit, which is characterized by the negative slope characteristic of wheel-rail adhesion.

In order to calculate the creep force under driving conditions, Polach [15] proposed a method, in which the negative slope characteristics of wheel-rail adhesion under larger creepage are taken into consideration, and a friction model related to sliding velocity was proposed as follows:

$$\mu = \mu_0[(1 - A)e^{-Bv} + A], \tag{15}$$

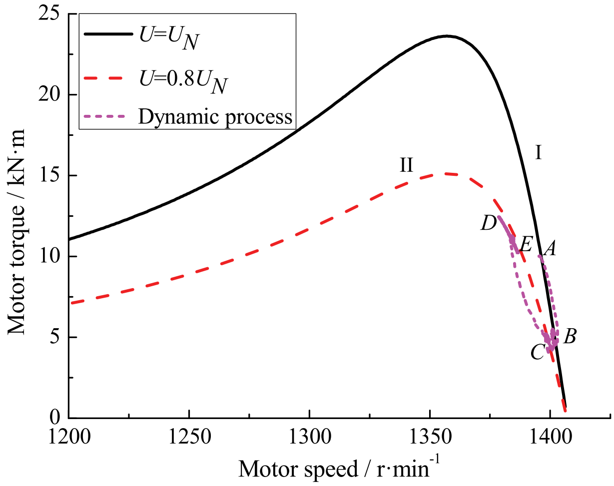

Figure 8. Mechanical characteristics of "the asynchronous traction motor.

where μ_0 is the maximum friction coefficient, v is the relative sliding velocity, A is the ratio of the friction coefficient corresponding to the infinite creepage and the maximum friction coefficient, and B is the friction exponential attenuation coefficient. Besides, in order to improve the applicability under large longitudinal slip and different contact conditions, the attenuation factors of Kalker coefficients in the adhesion area and sliding area are proposed, which are represented by k_A and k_S, respectively. By changing the k_A,k_S,μ_0, A, and B, the different adhesion characteristics corresponding to different wheel-rail contact states can be obtained. Typical model parameters for dry and wet conditions of the wheel-rail contact can be found in Ref. [2].

3.7. Electric drive system and control

The "AC-DC-AC" electric drive mode is adopted in high-power locomotives. The asynchronous traction motor model is established, and its mechanical characteristics are considered. Besides, the traction motor is operated with rated voltage and frequency. It should be noted that the model considers only the mechanical characteristics of the traction motor and does not use the adhesion control unit. As shown in Figure 8, curves *I* and *II* are different mechanical characteristics of the asynchronous traction motor with different voltages. The dynamic simulation is conducted by keeping the resistance constant and reducing the voltage at a certain time, and thus, the dynamic process of the motor is obtained and shown by the short dashed line. The traction motor experiences a process of "A-B-C-D-E," and it operates stably again at point E.

4. Stick-slip vibration characteristics

4.1. Simulation scenario

Two simulation scenarios are considered in this chapter. For the first scenario, the locomotive hauls the train running on a ramp, the slope and the traction weight of which are 6‰and 5000 t, respectively. The locomotive runs on a smooth straight track with a speed of 60 km/h, and thus, the resistance can be calculated using Equation 9. Controlling the traction torque by adjusting the motor voltage to ensure that the locomotive's traction force and the resistance are balanced, the train runs uniformly. The friction coefficient on the rail surface decreases from 0.4 to 0.25 to simulate a sudden deterioration of the adhesion condition and remains at 0.25 for about 1.2s and then recovers to 0.4 rapidly. The adhesion characteristics change under different contact conditions can be simulated. According to the analysis in chapter 2, the stick-slip vibration of the driving system will take place. Considering that the influences of the mechanical structure and bogie system parameters on stick-slip vibration of the driving system are mainly discussed in this article, thus, the locomotive's adhesion recovers with the help of traction motor's mechanical characteristics and the driving system's stiffness and damping, and the adhesion control algorithms are not considered.

For the second scenario, the train runs on a smooth straight track with a speed of 40 km/h. According to the locomotive tractive characteristic curve in Ref. [33], the traction effort is 370kN, and the resistance and traction effort are balanced. The motor torque remains constant by means of the constant torque control. The friction coefficient on the rail surface is 0.4 in the normal operation state, and it is 0.25, 0.2, and 0.55 to simulate the low adhesion state, very low adhesion state, and the effects of sand spreading measures, respectively. Different contact conditions can be simulated by changing the friction coefficient to investigate the influence on re-adhesion of locomotive. It experiences a process of "normal operation state-low adhesion state-sand spreading-normal operation state-very low adhesion state-sand spreading." It should be noted that the locomotive's adhesion recovers with the help of the driving system's stiffness and damping and the sand spreading measures and the adhesion control algorithms are not considered.

4.2. Simulation results analysis

The tangential force coefficient-slip dynamic curve and the motor torque-speed dynamic curve are obtained by dynamic simulation, which are shown in Figures 9 (a,b), respectively. It can be seen that when the friction coefficient decreases, the operating condition changes from *A* to *B*, which is located in the negative slope section. However, the state corresponding to condition *B* is unstable, the variation range of longitudinal slip lies in both the adhesion part and the slip part resulting from the small stiffness of the driving system, and thus, the stick-slip vibration occurs. The alternate stick and slip state is displayed, which can cause the vibration of the driving system to intensify, and the traction effort cannot be made full use of. If the readhesion performance of locomotives is excellent, the adhesion can recover quickly. The asynchronous traction motor has hard mechanical characteristics, and thus, the motor torque decreases sharply with the increase of angular velocity, which is favourable for the readhesion ability of locomotives. It is worth noting that the motor torque-speed dynamic curve exhibits a limit cycle when stick-slip vibration occurs, which implies that the reasonable matching of mechanical and electrical systems and the effective adhesion control are beneficial for the readhesion ability of locomotives.

The frequency components of wheelset's longitudinal and angular acceleration before and when the stick-slip vibration occurs are shown in Figures 9 (c) and (d), in which there are some prominent frequency components that are well worth noting. 24 Hz and 17.25 Hz correspond to the natural frequency of longitudinal and rotary vibration of the wheelset, and 34.5 Hz, 51.75 Hz, and 69 Hz correspond to the frequency doubling of natural frequency of wheelset's rotary vibration. Besides, 8.2 Hz corresponds to the two times of rotating frequency of the wheelset caused by the dynamic misalignment of coupling. By observing the frequency components of wheelset's acceleration when stick-slip vibration occurs, it is illustrated that the dominant frequency components for angular acceleration are natural frequency of wheelset rotary vibration and its doubling frequency, while for the longitudinal acceleration, the dominant frequency components are the natural frequency of wheelset longitudinal vibration and the natural frequency of wheelset rotary vibration and its doubling frequency. For the wheelset's longitudinal acceleration, the components of twice the natural frequency of rotary vibration is most notable. Besides, it is obvious that the vibration of the driving system

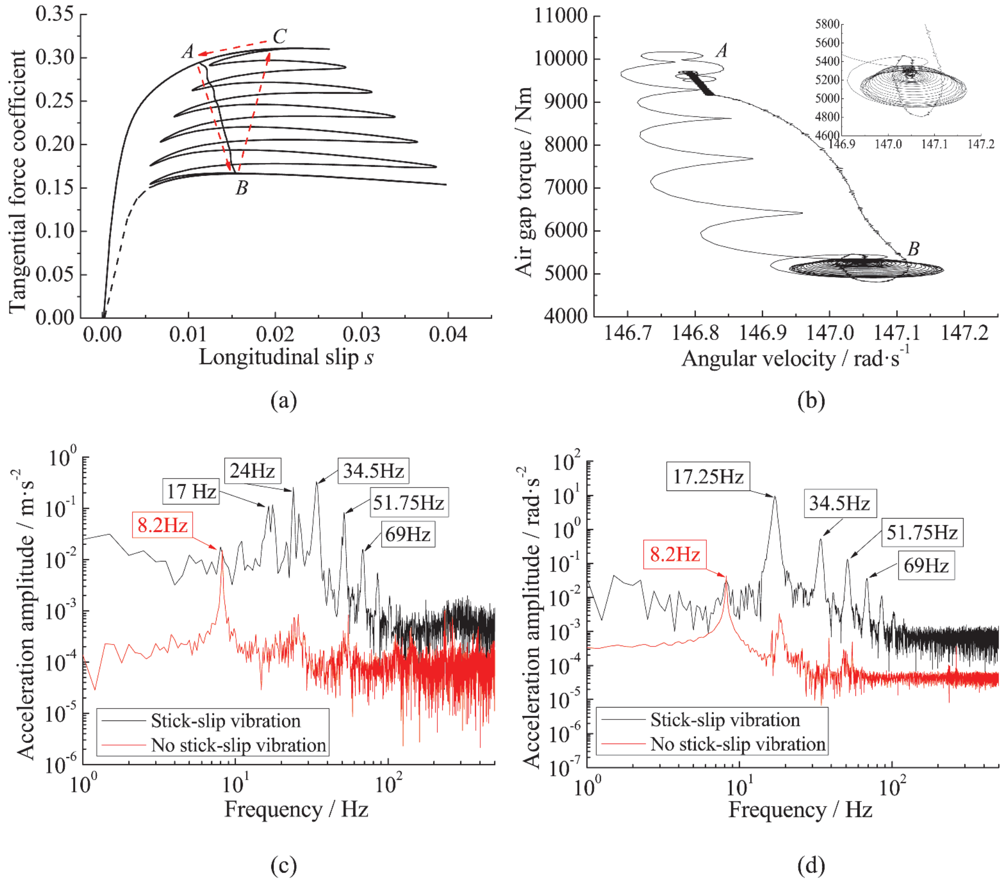

Figure 9. Simulation results for the first scenario: (a) tangential force coefficient-slip dynamic curve, (b) motor torque-speed dynamic curve, (c) amplitude spectrum of wheelset longitudinal acceleration, and (d) amplitude spectrum of wheelset angular acceleration.

intensifies when the stick-slip vibration occurs. It can be concluded that the stick-slip vibration is mainly characterized by the rotary and longitudinal natural vibration of the wheelset coupled by wheel-rail tangential force, which leads to some complex frequency components for the acceleration of the wheelset. The simulation results are consistent with the analysis in section 2.2. Moreover, it implies that the resonance of the driving system may occur as a result of unreasonable parameter matching of the bogie system.

For the second scenario, the simulation results are presented in Figure 10. It can be concluded that the friction condition has a significant influence on stick-slip vibration of the driving system, as well as the readhesion performance of locomotives. Once the stick-slip vibration occurs, the longitudinal slip will increase rapidly until the wheel idling occurs if there is no control measure. It illustrates that increasing the friction coefficient is an effective way for readhesion of locomotives, such as by means of sand spreading and other friction modifiers. It is noteworthy that the locomotive's adhesion will not recover immediately, and a short time is required for locomotive's readhesion even though the friction coefficient has recovered. Moreover, the required time for readhesion of locomotives is related to the vibration intensity, and this implies that in-time detected and control

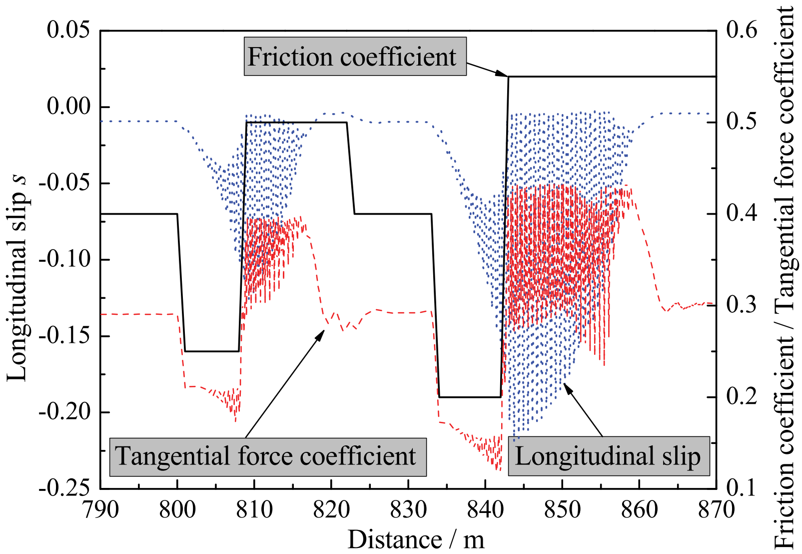

Figure 10. Simulation results for the second scenario.

measures are conducive to the readhesion of locomotive. Besides, the stick-slip vibration of the driving system can lead to the large fluctuation of longitudinal slip and tangential force coefficient, which is unfavourable for high traction effort.

5. Influencing factors of readhesion performance

The influencing factors for readhesion performance of locomotives are analysed in this chapter by simulation. The simulation conditions are consistent with the first scenario in section 4.1. The effects of track irregularity, gear backlash, rotor resistance of asynchronous traction motor, stiffness of six-bar double hollow shaft coupling, and motor suspension are discussed, as shown in Figure 11. It can be seen that the track irregularity and gear backlash have a less effect on stick-slip vibration, while the effects of stiffness of six-bar double hollow shaft coupling and motor suspension and rotor resistance are remarkable.

As shown in Figure 11(c), the wheel-rail contact changes to the slip state when the friction coefficient decreases on condition that a smaller stiffness of six-bar double hollow shaft coupling is adopted and the larger slip variation range makes it easier to go into the stick-slip state. The variation ranges of slip decrease with the increasing stiffness of six-bar double hollow shaft coupling, that is to say, if a larger stiffness is adopted, for example, 30 MN m/rad, the slip enters into full slip state after the friction coefficient decreases and cannot enter the adhesion area, the adhesion recovers when the friction coefficient restores, and thus, the stick-slip vibration will not occur. In addition, a conclusion can be drawn that a larger stiffness of six-bar double hollow shaft coupling is adopted, and the more quickly to restore adhesion, and the higher the locomotive traction capacity.

The effects of rotor resistance on stick-slip vibration are shown in Figure 11(d). It can be seen that it is easy to go into the sliding state when the friction coefficient decreases, and then the larger energy makes it easier to go into the stick-slip state if the asynchronous motor with softer mechanical characteristics is adopted. Moreover, it is unfavourable for the recovery of adhesion. It is revealed that adopting the asynchronous motor with hard mechanical characteristics can narrow the variation ranges of slip, which is conducive to improving the locomotive traction capacity.

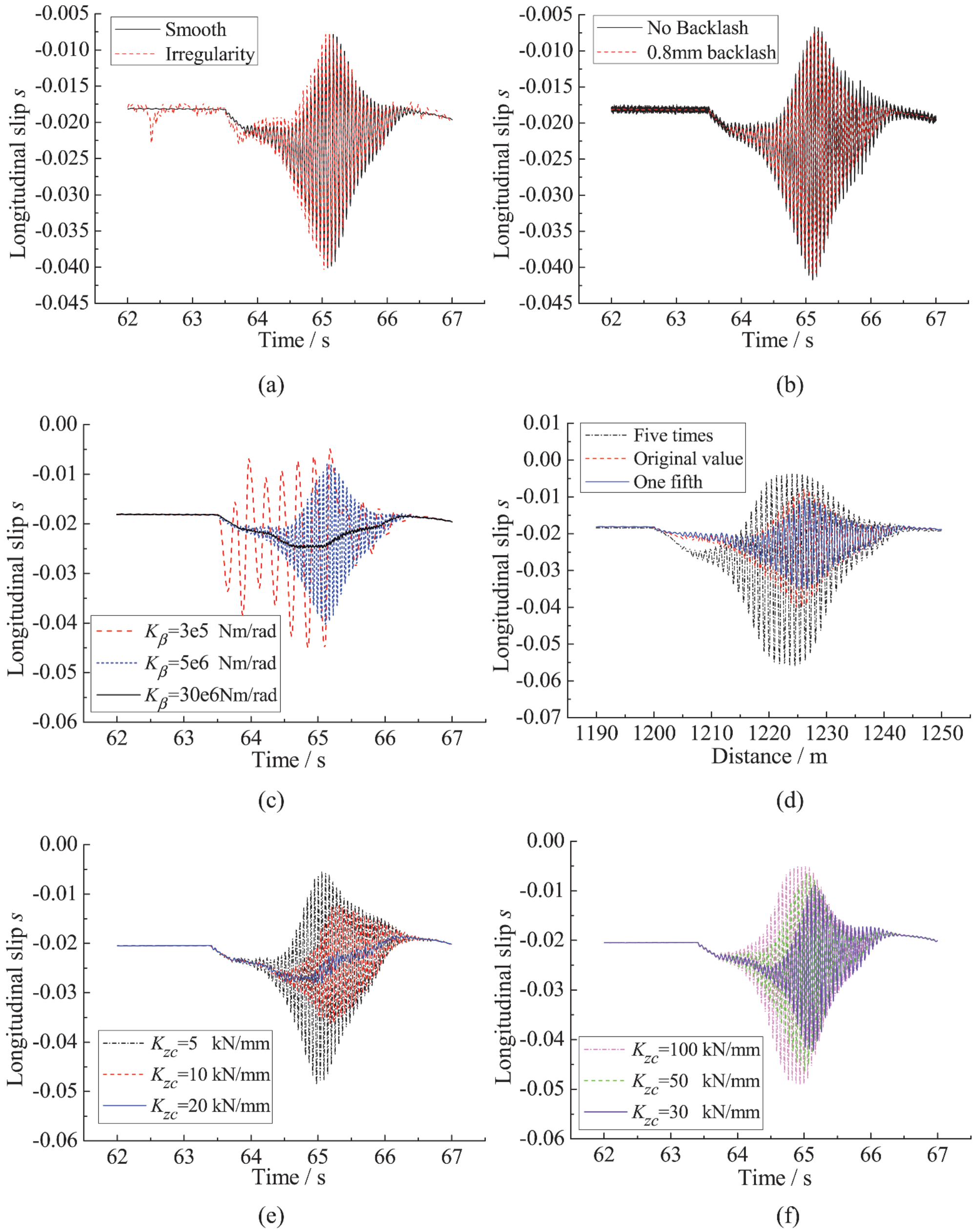

Figure 11. Influencing factors of readhesion performance: (a) track irregularity, (b) gear backlash, (c) Stiffness of six-bar double hollow shaft coupling, (d) rotor resistance, (e) smaller motor suspension stiffness, and (f) larger motor suspension stiffness.

The slip with different motor suspension stiffness values is shown in Figure 11(e,f). It is demonstrated that increasing the stiffness of motor suspension is favourable for stick-slip vibration within a certain range. However, the stiffness of motor suspension is not as larger as better. That is, there is the optimal stiffness for motor suspension. For example, if the stiffness of motor suspension is 20 kN/mm, the slip directly enters the sliding area after the friction coefficient decreases and quickly changes into the stick state when the friction coefficient recovers, and thus, the stick-slip vibration does not occur, while upon further increasing the motor suspension stiffness, it is unfavourable as the interaction vibration between the bogie frame and the driving system is enhanced.

6. Resonance analysis

According to the analysis in chapter 4, the rotary and longitudinal vibrations of the wheelset are coupled by wheel-rail tangential force, resulting in some complex frequency components when stick-slip vibration occurs. The resonance analysis is conducted in this chapter by matching the primary longitudinal stiffness with different six-bar double hollow shaft coupling stiffness. Two conditions are taken into consideration, for which the primary longitudinal stiffness is represented by K_{px} are 37.4 kN/mm and 15 kN/mm, respectively. It is worth noting that the motor torque remains constant by means of the constant torque control in this chapter to clarify the effects of structural stiffness more clearly. The friction coefficient on the rail surface decreases to simulate the poor adhesion conditions, and then it increases as a result of adopting sand spreading measures. Assume that the initial friction coefficient is 0.4, decreases to 0.25 at one moment and remains for a while, and then recovers to 0.5 to simulate the effects of sand spreading measures.

The longitudinal slips corresponding to different matching of primary longitudinal stiffness with six-bar double hollow shaft coupling stiffness are shown in Figures 12 and 13. In general, a larger stiffness of six-bar double hollow shaft coupling is conducive to the readhesion ability of the locomotive. However, more attention should be paid to the condition of 10 MN m/rad of six-bar double hollow shaft coupling stiffness in Figure 12 and 1 MN·m/rad and 4 MN m/rad of six-bar double hollow shaft coupling stiffness in Figure 13. The amplitude of longitudinal slip is larger and the adhesion recovery time is longer, which indicates that the stick-slip vibration is more severe. For the condition of 37.4 kN/mm of primary longitudinal stiffness matching with different six-bar double hollow shaft coupling stiffness, the longitudinal and angular acceleration of the wheelset is shown in Figure 14. Besides, the frequency components corresponding to the matching of 37.4 kN/mm of primary longitudinal stiffness with different six-bar double hollow shaft coupling stiffness characterizing the conditions of without and with resonance occurrence are shown in Figure 15. There are several remarkable frequency components in Figure 15(b), which correspond to the natural frequencies of longitudinal and rotary vibration of the wheelset, which are 24 Hz and 23 Hz, respectively. It can be concluded that the resonance occurs if

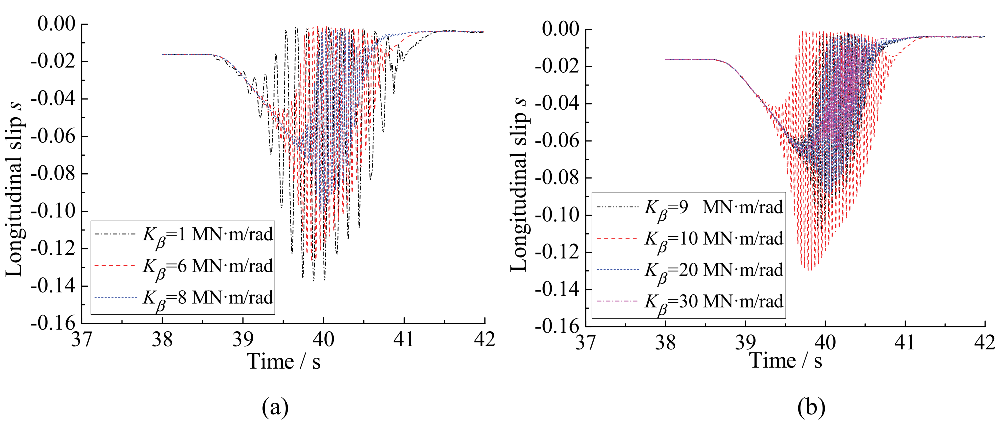

Figure 12. Longitudinal slip with different hollow shaft coupling stiffness (K_{px} = 37.4 kN/mm): (a) smaller hollow shaft coupling stiffness and (b) larger hollow shaft coupling stiffness.

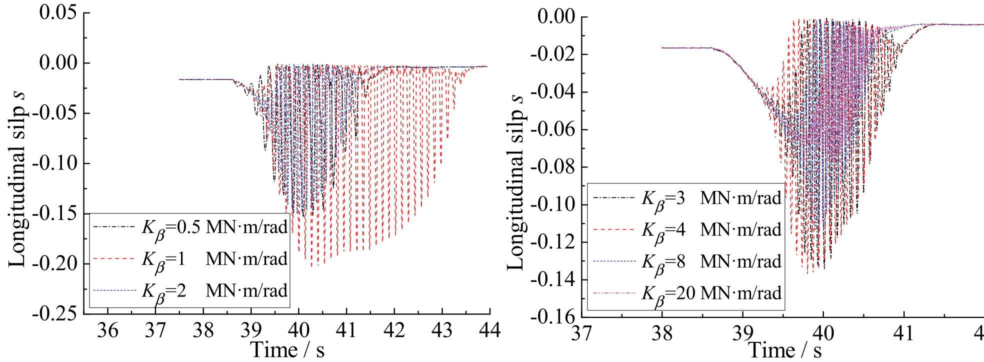

(a) (b)

Figure 13. Longitudinal slip with different hollow shaft coupling stiffness (K_{px} = 15 kN/mm): (a) smaller hollow shaft coupling stiffness and (b) larger hollow shaft coupling stiffness.

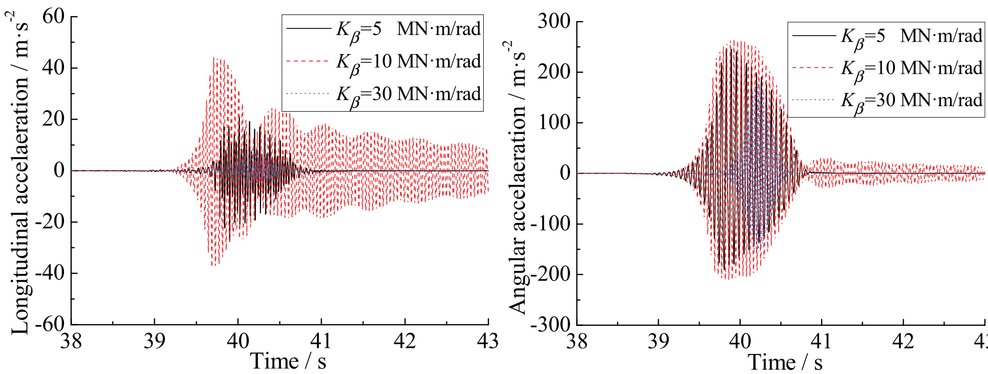

(a) (b)

Figure 14. Acceleration of the wheelset with different hollow shaft coupling stiffness (K_{px} = 37.4 kN/mm): (a) longitudinal acceleration and (b) angular acceleration.

the natural frequencies of longitudinal and rotary vibration of the wheelset are close, which will cause the stick-slip vibration to intensify, and it is unfavourable for the readhesion ability of the locomotive.

Similarly, for the condition of 4 MN m/rad of six-bar double hollow shaft coupling stiffness matching with a primary longitudinal stiffness of 15 kN/mm, the natural frequencies of longitudinal and rotary vibration of the wheelset are close, and thus, the resonance occurs. Besides, for the condition of the six-bar double hollow shaft coupling stiffness of 1 MN·m/rad matching with the primary longitudinal stiffness of 15 kN/mm, the natural frequency of longitudinal vibration of the wheelset is twice the rotary vibration and the resonance occurs as well.

It signifies that reasonable parameters matching to avoid the resonance is of significance during the design process of locomotive. As for the locomotive with a bogie frame suspension driving system, reasonable matching of six-bar double hollow shaft coupling stiffness and primary longitudinal stiffness is especially important.

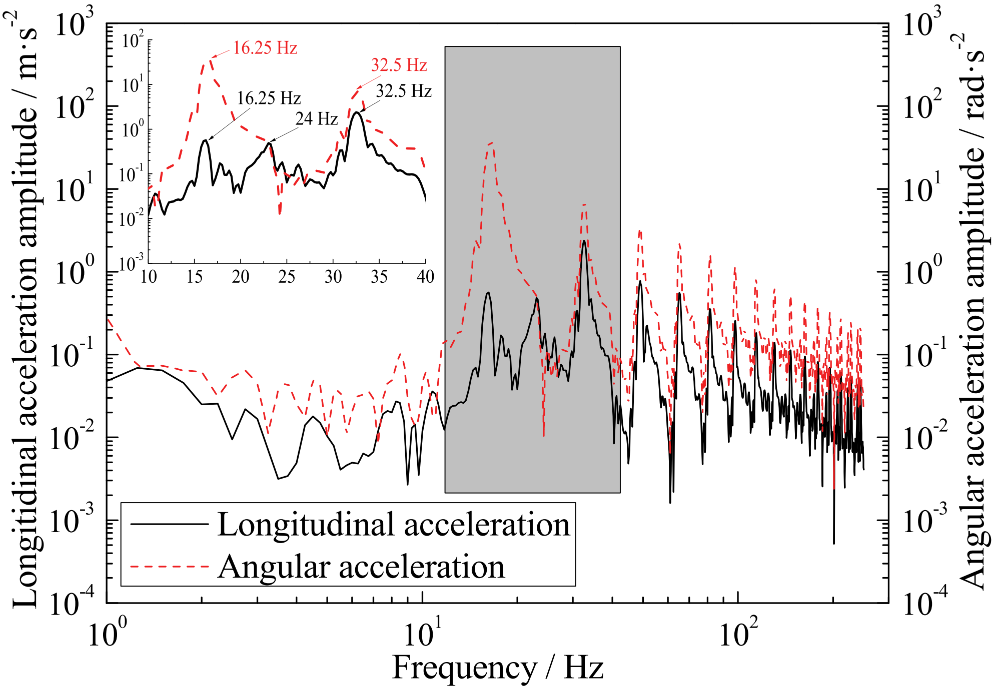

(a)

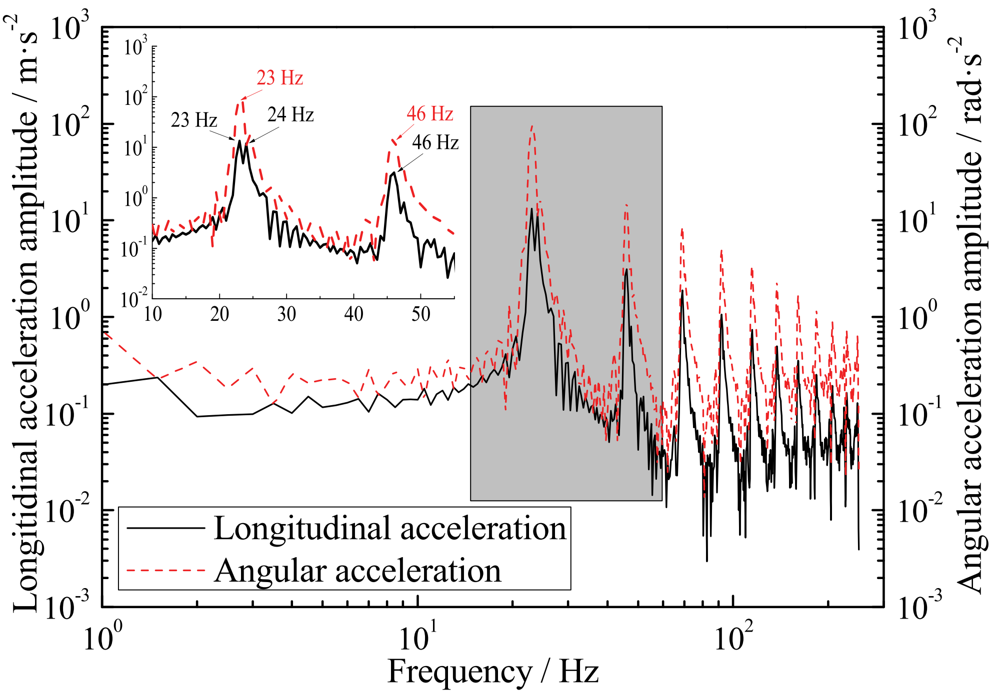

(b)

Figure 15. Acceleration amplitude spectrum (K_{px} = 37.4 kN/mm): (a) K_β = 5 MN·m/rad with no resonance occurrence and (b) K_β = 10 MN·m/rad with resonance occurrence.

7. Conclusion

(1) The stick-slip vibration occurrence conditions of locomotives with a bogie frame driving system was analysed based on the dynamic slip and the mechanical characteristics of the motor. There are more flexible connection mechanisms in the bogie frame driving system compared with nose-suspended, which is unfavourable for the readhesion performance of locomotives. The longitudinal and rotary vibrations of the wheelset are coupled by tangential force, and the vibration-dominant frequency is more complex, which may lead to system resonance when the stick-slip vibration occurs.

(2) The influencing factors for readhesion performance of locomotives were analysed by simulation. It can be concluded that the track irregularity and gear backlash have less effects on the readhesion ability of locomotives. Besides, the effects of torsional stiffness of six-bar double hollow shaft coupling and the vertical stiffness of motor suspension, as well as the longitudinal stiffness of primary suspension, are remarkable. Increasing the structure stiffness is conducive to decreasing the dynamic slip rate, which is favourable for the readhesion performance of locomotives. It is worth noting that increasing the stiffness of motor suspension within a certain range is favourable, while it is not as larger as better, and there is the optimal stiffness for motor suspension. Moreover, adopting the asynchronous motor with hard mechanical characteristics is also an effective way.

(3) The resonance in the driving system of locomotives with bogie frame suspension was analysed. As the weakness of the bogie frame suspension driving system, the stiffness of six-bar double hollow shaft coupling is of great significance. The resonance occurs if the wheelset's natural frequency of longitudinal vibration is close to rotary vibration frequency or its frequency doubling, that is, the unreasonable matching of primary longitudinal stiffness and six-bar double hollow shaft coupling stiffness can result in the resonance of the driving system, which may cause the vibration to intensify, and it is unfavourable for the readhesion performance of locomotives.

Disclosure statement

No potential conflict of interest was reported by the author(s).

Funding

The material in this paper is based on the work supported by grants (51675443 and 51735012) from the National Natural Science Foundation of China and National Railway Group Science and Technology Program grant (N2020J026 and N2021J028) and Traction Power State Key Laboratory grant (2022TPL_Q02) of the Independent Research and Development Projects..

References

[1] Zhang WH, Chen JZ, Wu XJ, et al. Wheel/rail adhesion and analysis by using full scale roller rig. Wear. 2002;253(1–2):82–88.
[2] Polach O. Creep force in simulation of traction vehicles running on adhesion limit. Wear. 2005;258(7–8):992–1000.
[3] Vollebregt EAH. Numerical modeling of measured railway creep versus creep-force curves with CONTACT. Wear. 2014;314(1):87–95.
[4] Frohling R, Spangenberg U, Reitmann E. Root cause analysis of locomotive wheel tread polygonisation. Wear. 2019;432–433:102911.
[5] Kalousek J, Johnson KL. An investigation of short pitch wheel and rail corrugations on the Vancouver mass transit system. Proc Inst Mech Eng Part F. 1992;206(2):127–135.
[6] Zhao XN, Chen GX, Lv JZ, et al. Study on the mechanism for the wheel polygonal wear of high speed trains in terms of the frictional self-excited vibration theory. Wear. 2019;426(B):1820–1827.

[7] Tao GQ, Wen ZF, Jin XS, et al. Polygonisation of railway wheels: a critical review. Railway Eng Sci. 2020;28(4):317–345.
[8] Wang WJ, Shen P, Song JH, et al. Experimental study on adhesion behavior of wheel/rail under dry and water conditions. Wear. 2011;271(9–10):2699–2705.
[9] Olofsson U, Sundvall K. Influence of leaf, humidity and applied lubrication on friction in the wheel-rail contact: pin-on-disc experiments. Proc Inst Mech Eng Part F-J Rail Rapid Transit. 2004;218(1):235–242.
[10] Hirotsu T, Kasai S, Takai H. Self-excited vibration during slippage of parallel Cardan drives for electric railcars. JSME Int J. 1987;30(266):1304–1310.
[11] Muller S, Kogel R. Numerical simulation of roll-slip oscillations in locomotive drives. ZAMM-Z Angew Math Mech. 2001;81(supl):61–64.
[12] Wu YF. Stability analysis of the vibration of the frame-mounted motor driving system. J Chin Railway Soc. 1992;14(2):1–7. (in Chinese).
[13] X SUN. The locomotive system design of high adhesion performance. J Southwest Jiaotong Univ. 1994;29(3):235–247. (in Chinese).
[14] Polach O. Influence of locomotive tractive effort on the forces between wheel and rail. Veh Syst Dyn. 2001;35(supl):7–22.
[15] Polach O. A fast wheel-rail force calculation computer code. Veh Syst Dyn. 1999;33(supl):728–739.
[16] Lata M. The modern wheelset drive system and possibilities of modeling the torsion dynamics. Transport. 2008;23(2):172–181.
[17] Lata M, Voltr P. Identification of transient phenomena occurring at the initiation and termination of wheelset sliding. Transport. 2012;27(1):86–91.
[18] Liu S, Tian Y, Daniel WJT, et al. Modelling of track wear damage due to changes in friction conditions: a comparison between AC and DC electric drive locomotives. Wear. 2016;366:338–345.
[19] Chen ZG, Zhai WM, Wang KY. Locomotive dynamic performance under traction/braking conditions considering effect of gear transmissions. Veh Syst Dyn. 2018;56(7):1097–1117.
[20] Chen ZG, Zhai WM, Wang KY. A locomotive–track coupled vertical dynamics model with gear transmissions. Veh Syst Dyn. 2017;55(2):244–267.
[21] Liu YQ, Chen ZG, Li W, et al. Dynamic analysis of traction motor in a locomotive considering surface waviness on races of a motor bearing. Railway Eng Sci. 2021;29(4):379–393.
[22] Liu YQ, Chen ZG, Zhai WM, et al. Dynamic investigation of traction motor bearing in a locomotive under excitation from track random geometry irregularity. Int J Rail Transp. 2022;10(1):72–94.
[23] Ren ZS, Xin X, Sun G, et al. The effect of gear meshing on the high-speed vehicle dynamics. Veh Syst Dyn. 2021;59(5):743–764.
[24] Huang GH, Xu SS, Zhang WH, et al. Super-harmonic resonance of gear transmission system under stick-slip vibration in high-speed train. J Cent South Univ. 2017;24(3):726–735. (in Chinese).
[25] Spiryagin M, Wolfs P, Szanto F, et al. Simplified and advanced modelling of traction control systems of heavy-haul locomotives. Veh Syst Dyn. 2015;53(5):672–691.
[26] Spiryagin M, Lee KS, Yoo HH. Control system for maximum use of adhesive forces of a railway vehicle in a tractive mode. Mech Syst Signal Pr. 2008;22(3):709–720.
[27] Spiryagin M, Wolfs P, Cole C, et al. Influence of AC system design on the realisation of tractive efforts by high adhesion locomotives. Veh Syst Dyn. 2017;55(8):1241–1264.
[28] Spiryagin M, Wu Q, Polach O, et al. Problems, assumptions and solutions in locomotive design, traction and operational studies. Railway Eng Sci. 2022. DOI:10.1007/s40534-021-00263-w.
[29] Spiryagin M, Cole C, Sun YQ. Adhesion estimation and its implementation for traction control of locomotives. Int J Rail Transp. 2014;2(3):187–204.
[30] Yao Y, Zhang HJ, Luo SH. An analysis of resonance effects in locomotive drive systems experiencing wheel/rail saturation adhesion. Proc Inst Mech Eng Part F. 2014;228(1):4–15.
[31] Yao Y, Zhang HJ, Li YM, et al. The dynamic study of locomotives under saturated adhesion. Veh Syst Dyn. 2011;49(8):1321–1338.
[32] Yao Y, Zhao SY, Xiao FX, et al. The effects of wheelset driving system suspension parameters on the re-adhesion performance of locomotives. Veh Syst Dyn. 2015;53(12):1935–1951.
[33] TB/T 1407.1-2018. Railway train traction calculation Part 1: trains with locomotives. Beijing: Chinese Railways; 2018. (in Chinese).
[34] German Standards Committees. Calculation of load capacity of cylindrical gears: introduction and general influence factors (DIN3990-1-1987). Technical Report. Berlin: German Institute for Standardization, 1987.
[35] Ma WH, Song RR, Jie CA, et al. Influences of buffer impedance characteristics on dynamics performances for heavy haul train. J Traff Transp Eng. 2011;11(2):59–64. (in Chinese).

Appendix

Table A1. Main parameters of the locomotive's dynamic model.

Parameters	Value
Axle load (t)	30
Bogie wheelbase (mm)	2900
Distance between bogie centres (mm)	9000
Wheel rolling radius (mm)	625
Mass of the wheelset (kg)	3138
Roll inertia of the wheelset (kg m^2)	2230
Pitch inertia of the wheelset (kg m^2)	440
Yaw inertia of wheelset (kg m^2)	2244
Mass of the car body (kg)	76,900
Roll inertia of the car body (kg m^2)	1.202e5
Pitch inertia of the car body (kg m^2)	1.928e6
Yaw inertia of the car body (kg m^2)	1.922e6
Mass of the bogie frame (kg)	6032
Roll inertia of the bogie frame (kg m^2)	16,967
Pitch inertia of the bogie frame (kg m^2)	14,415
Yaw inertia of the bogie frame (kg m^2)	27,813
Longitudinal axle guidance stiffness per axle box (kN mm^{-1})	37.4
Primary lateral stiffness per axle box (kN mm^{-1})	7.961
Primary vertical stiffness per axle box (kN mm^{-1})	2.309
Primary vertical damping coefficient per axle box (kN s/m)	43.5
Secondary longitudinal stiffness (single, six sets for each bogie) (kN mm^{-1})	0.291
Secondary lateral stiffness (single, six sets for each bogie) (kN mm^{-1})	0.291
Secondary vertical stiffness (single, six sets for each bogie) (kN mm^{-1})	0.632
Secondary lateral damping coefficient (kN s/m)	60.1
Secondary vertical damping coefficient (kN s/m)	89.2